INSTITUTE FOR FUSION STUDIES

DE-FG03-96ER-54346-749 IFSR #749

High-Mode-Number Ballooning Modes in a Heliotron/Torsatron System: I. Local Magnetic Shear

N. NAKAJIMA[a)]
Institute for Fusion Studies
The University of Texas at Austin
Austin, Texas 78712 USA

[a)]Permanent address: National Institute for Fusion Science, Nagoya 464-01, Japan

May 1996

THE UNIVERSITY OF TEXAS

AUSTIN

DISCLAIMER

High-mode-number ballooning modes in a heliotron/torsatron system: I. Local magnetic shear

N. Nakajima[a)]

Institute for Fusion Studies, The University of Texas at Austin

Austin, Texas 78712 USA

Abstract

The characteristics of the local magnetic shear, a quantity associated with high-mode-number ballooning mode stability, are considered in heliotron/torsatron devices that have a large Shafranov shift. The local magnetic shear is shown to vanish even in the stellarator-like region in which the global magnetic shear $s \equiv 2\frac{d\ln\iota}{d\ln\psi}$ (ι is the global rotational transform and $2\pi\psi$ is the toroidal flux) is positive. The reason for this is that the degree of the local compression of the poloidal magnetic field on the outer side of the torus, which maintains the toroidal force balance, is reduced in the stellarator-like region of global magnetic shear because the global rotational transform in heliotron/torsatron systems is a radially increasing function. This vanishing of the local magnetic shear is a universal property in heliotron/torsatron systems with a large Shafranov shift since it results from toroidal force balance in the stellarator-like global shear regime that is inherent to such systems.

PACS: 52.35.Py, 52.55.Hc

[a)]Permanent address:*National Institute for Fusion Science, Nagoya 464-01, Japan*

I. INTRODUCTION

In currentless helical systems with a planar axis, such as heliotron/torsatron devices, the global rotational transform ι of the vacuum magnetic field increases in the minor radius direction, i.e., the global shear defined as $s \equiv 2\frac{d\ln\iota}{d\ln\psi}$ is positive ($2\pi\psi$ is the toroidal flux). This is in contrast to the tokamak for which the global magnetic shear is usually negative ($s < 0$). (Note that in a tokamak, the definition $s \equiv 2\frac{d\ln\iota^{-1}}{d\ln\psi}$ is used for the global shear, and hence it has the opposite sign to that in a helical system.) Using a low-β approximation (where β is the ratio of the kinetic pressure to the magnetic pressure), Shafranov[1] speculated that if the global shear is stellarator-like, i.e., positive ($s > 0$), then high-mode-number ballooning modes would not become unstable when the Mercier modes are stable. A counter-example to Shafranov's conjecture was found, however, in a Heliac configuration.[2] With the use of a low-β approximation and a steep-gradient equilibrium model, it was pointed out that the averaged Pfirsch-Schlüter current can make the global magnetic shear change sign, so that unstable high-mode-number ballooning modes will occur in the resultant tokamak-like global magnetic shear regime.[3] Using three-dimensional equilibria, Cooper *et al.*[4] found high-mode-number ballooning modes in the stellarator-like global magnetic shear regime of the ATF device; however, they did not give the physical mechanism.

In currentless heliotron/torsatron systems that allow an inherently large Shafranov shift as a result of toroidal force balance, the characteristics of the vacuum configuration—e.g., the global and local pitch of the magnetic field, and the global shape of the flux surfaces—can be significantly deformed as the plasma beta increases. Thus, the low-β approximation and the steep-gradient model may not be applicable to such systems. In this paper, we investigate the properties of the local magnetic shear using a general magnetic coordinate system. We find that in the stellarator-like (i.e., positive global magnetic shear) region of heliotron/torsatron

systems with a large Shafranov shift, it is possible for high-mode-number ballooning modes to be unstable, because the stabilizing effect of field line bending is reduced, even though this region is Mercier stable.

The present paper is organized as follows. In Sec. II, expressions for the local magnetic shear[5] and the perpendicular wave number for the high-mode-number ballooning mode equation are given in various magnetic coordinate systems. Although the Boozer coordinate system[6] will be used for our numerical calculations, a new magnetic coordinate system related to the Boozer coordinate system is introduced for the analytical calculations. The characteristics of the local magnetic shear are described in Sec. III. Numerical calculations and an analytical treatment are used to explain why the local magnetic shear disappears in the stellarator-like region of positive global shear. A model expression for the local magnetic shear is also presented. Concluding comments and discussion are given in Sec. IV.

II. EXPRESSIONS FOR THE LOCAL MAGNETIC SHEAR

The vector form of the incompressible high-mode-number ballooning mode equation[7] is

$$\mathbf{B}\cdot\nabla\left[\frac{|\mathbf{k}_\perp|^2}{B^2}\mathbf{B}\cdot\nabla\Psi\right]+\frac{\rho_m}{B^2}\omega^2|\mathbf{k}_\perp|^2\Psi+\frac{2}{B^2}\hat{n}\times\mathbf{k}_\perp\cdot\kappa\hat{n}\times\mathbf{k}_\perp\cdot\nabla P\Psi=0, \tag{1}$$

where $\mathbf{k}_\perp$ is the perpendicular wave number, $\hat{n}=\frac{\mathbf{B}}{B}$ the unit vector along the field line, κ the magnetic curvature, ρ_m the mass density, and P the pressure. The potential energy corresponding to the variational form of Eq. (1), namely,

$$\delta W=\frac{1}{2}\int d\tau\left[|\mathbf{k}_\perp|^2\left(\hat{n}\cdot\nabla\Psi\right)^2-\frac{2}{B^2}\hat{n}\times\mathbf{k}_\perp\cdot\kappa\hat{n}\times\mathbf{k}_\perp\cdot\nabla P\Psi^2\right]. \tag{2}$$

exhibits the competition between the stabilizing effect of field line bending, represented by $|\mathbf{k}_\perp|^2$, and the destabilizing effect of the pressure gradient when the magnetic curvature is unfavorable.

The magnitude of the perpendicular wave number, $|\mathbf{k}_\perp|$, is so closely related to the local magnetic shear[5] that the characteristics of the local magnetic shear have a direct bearing

on whether high-mode-number ballooning modes are stable. For studies of the local magnetic shear that involve numerical stability calculations of the high-mode-number ballooning modes, it is appropriate to use the Boozer coordinate system,[6] at least for three-dimensional equilibria. For an analytical treatment, however, the Boozer coordinate system may not necessarily be the most suitable for finite-β three-dimensional equilibria with large Shafranov shifts, since almost all the information about changes in the local magnetic structure that result from the Shafranov shift are expressed by metrics that are difficult to handle analytically. Thus, in what follows, we will introduce more general magnetic coordinate systems in which the magnetic field lines are not straight. We will show later that the defect of not having straight field lines is what allows us to handle the local magnetic shear analytically and clarify its properties.

Let us introduce a general magnetic coordinate system (ψ, θ, ζ) such that the contravariant and covariant expressions of the magnetic field are given, respectively, by

$$\mathbf{B} = \nabla\psi \times \nabla[\theta - \iota\zeta + \lambda(\psi, \theta, \zeta)] \tag{3}$$

and

$$\mathbf{B} = \nabla[J\zeta + I\theta + \omega(\psi, \theta, \zeta)] + [-\dot{J}\zeta - \dot{I}\theta + \beta(\psi, \theta, \zeta)]\nabla\psi. \tag{4}$$

Here $\psi = \frac{\Phi_T}{2\pi}$ is the label of the flux surface with Φ_T the toroidal flux inside a flux surface; derivatives are denoted as $\dot{J} \equiv \frac{dJ}{d\psi}$; θ and ζ are the poloidal and toroidal angles; and $2\pi J$ is the poloidal current outside a flux surface and $2\pi I$ the toroidal current inside. The three functions λ, ω, and β are periodic functions with respect to θ and ζ. The periodic function β must satisfy the following magnetic differential equation:

$$\mathbf{B} \cdot \nabla\beta = \dot{P} + \frac{1}{\sqrt{g}}\left\{\dot{J}(1 + \partial_\theta\lambda) + \dot{I}(\iota - \partial_\zeta\lambda)\right\}, \tag{5}$$

where $\sqrt{g}$ is the Jacobian,

$$\sqrt{g} = \frac{1}{\nabla\psi \cdot \nabla\theta \times \nabla\zeta} = \frac{(1 + \partial_\theta\lambda)(J + \partial_\zeta\omega) + (\iota - \partial_\zeta\lambda)(I + \partial_\theta\omega)}{B^2}. \tag{6}$$

From the solvability condition of Eq. (5) and the flux surface average of Eq. (6), the following two relations are obtained:

$$\dot{P} = -(2\pi)^2 \frac{\dot{J} + \iota \dot{I}}{\dot{V}}, \tag{7}$$

$$\left\langle B^2 \right\rangle = \tag{8}$$

$$(2\pi)^2 \frac{J + \iota I}{\dot{V}}. \tag{9}$$

Here, V is the volume surrounded by the flux surface ψ, and brackets indicate a flux surface average:

$$\langle f \rangle = \frac{d}{dV} \int f d\tau. \tag{10}$$

For the high-mode-number ballooning mode equation, Eq. (1), it is convenient to use a field-line coordinate system (ψ, η, α), which is related to the above magnetic coordinate system (ψ, θ, ζ) through

$$\begin{aligned} \eta &= \theta, \\ \alpha &= \zeta - \tfrac{1}{\iota}\theta - \tfrac{1}{\iota}\lambda(\psi, \theta, \zeta). \end{aligned} \tag{11}$$

In the field-line coordinate system (ψ, η, α), the perpendicular wave number $|\mathbf{k}_\perp|$ is expressed in terms of an integral of the local magnetic shear $\hat{s}$ along the magnetic field line, as follows:

$$|\mathbf{k}_\perp|^2 = \frac{2\psi B^2}{B_0 |\nabla\psi|^2} \left\{ 1 + \left(\frac{|\nabla\psi|^2}{2\psi B} \right)^2 \left[\int^\eta \hat{s} d\eta \right]^2 \right\}. \tag{12}$$

Here the local magnetic shear can be decomposed into two parts as

$$\hat{s} = \frac{2\psi\sqrt{g}}{\iota} \frac{\mathbf{B} \times \nabla\psi}{|\nabla\psi|^2} \cdot \nabla \times \left[\frac{\mathbf{B} \times \nabla\psi}{|\nabla\psi|^2} \right] = s + \tilde{s}, \tag{13}$$

with

$$s \equiv \frac{2\psi}{\iota} \frac{d\iota}{d\psi}, \tag{14}$$

$$\tilde{s} = \frac{\partial}{\partial\eta} \left\{ -2\psi\iota\partial_\psi \left(\frac{\lambda}{\iota} \right) + 2\psi \frac{(J + \partial_\zeta\omega) g_{\psi\theta} - (I + \partial_\theta\omega) g_{\psi\zeta}}{\sqrt{g} |\nabla\psi|^2} \right\}. \tag{15}$$

The integral of the local magnetic shear yields

$$\int^{\eta} \widehat{s} d\eta = s(\eta - \theta_k) - 2\psi \iota \partial_\psi \left(\frac{\lambda}{\iota}\right) + 2\psi \frac{(J + \partial_\zeta \omega) g_{\psi\theta} - (I + \partial_\theta \omega) g_{\psi\zeta}}{\sqrt{g} |\nabla \psi|^2}, \tag{16}$$

where the radial wave number θ_k is the constant of integration, and the covariant metrics are given by

$$g_{\psi\theta} = \partial_\psi \mathbf{r} \cdot \partial_\theta \mathbf{r}, g_{\psi\zeta} = \partial_\psi \mathbf{r} \cdot \partial_\zeta \mathbf{r}. \tag{17}$$

The local magnetic shear $\widehat{s}$ consists of the global magnetic shear s and an oscillatory component $\widetilde{s}$. Note that the derivative of $\frac{\lambda}{\iota}$ with respect to ψ appears in $\widetilde{s}$, the oscillatory part of the local magnetic shear; this comes from the last term on the right-hand side of Eq. (10) and means that the magnetic field lines are not straight in this magnetic coordinate system. For subsequent use, we give the expression for the $g_{\theta\theta}$ metric element:

$$g_{\theta\theta} = \partial_\theta \mathbf{r} \cdot \partial_\theta \mathbf{r} = \frac{(I + \partial_\theta \omega)^2 + (1 + \partial_\theta \lambda)^2 |\nabla \psi|^2}{B^2} > 0. \tag{18}$$

In the Boozer coordinate system[6] $(\psi, \theta_B, \zeta_B)$, the contravariant and covariant expressions of the magnetic field are given, respectively, by

$$\mathbf{B} = \nabla \psi \times \nabla (\theta_B - \iota \zeta_B), \tag{19}$$

$$\mathbf{B} = \nabla (J \zeta_B + I \theta_B) + (-\dot{J} \zeta_B - \dot{I} \theta_B + \beta_B) \nabla \psi. \tag{20}$$

The transformation from the general magnetic coordinate system (ψ, θ, ζ) to the Boozer coordinate system is obtained from the solution of the following relations:

$$\theta_B - \iota \zeta_B = \theta - \iota \zeta + \lambda(\psi, \theta, \zeta), \tag{21}$$

$$J \zeta_B + I \theta_B = J \zeta + I \theta + \omega(\psi, \theta, \zeta). \tag{22}$$

The single-valuedness of the magnetic field $\mathbf{B}$ with respect to θ and ζ, which is expressed by

$$\theta_B = \theta + p_T(\psi, \theta, \zeta), \tag{23}$$

$$\zeta_B = \zeta + q_T(\psi, \theta, \zeta), \tag{24}$$

where the functions p_T and q_T are periodic functions with respect to θ and ζ, must be taken into account. By substituting Eqs. (22) and (23) into Eqs. (20) and (21), we find that the functions p_T and q_T are given by

$$p_T(\psi,\theta,\zeta) = \frac{J\lambda(\psi,\theta,\zeta) + \iota\omega(\psi,\theta,\zeta)}{J + \iota I}, \tag{25}$$

$$q_T(\psi,\theta,\zeta) = \frac{-I\lambda(\psi,\theta,\zeta) + \omega(\psi,\theta,\zeta)}{J + \iota I}. \tag{26}$$

Equations (22)–(25) provide the prescription for transforming from the general magnetic coordinate system (ψ,θ,ζ) to the Boozer coordinate system (ψ,θ_B,ζ_B).

If the general magnetic coordinate system (ψ,θ,ζ) happens to be identical to the Boozer coordinate system, then p_T and q_T must vanish in Eqs. (22) and (23), i.e., $\lambda = \omega = 0$ from Eqs. (24) and (25). In this case the field-line coordinate system (ψ,η_B,α_B) is related to the Boozer coordinate system (ψ,θ_B,ζ_B) through

$$\begin{aligned} \eta_B &= \theta_B, \\ \alpha_B &= \zeta_B - \tfrac{1}{\iota}\theta_B. \end{aligned} \tag{27}$$

Hence, we obtain the expressions for the perpendicular wave number and other associated quantities in the field-line coordinate system by putting $\lambda = \omega = 0$ in Eqs. (11)–(17):

$$|\mathbf{k}_\perp|^2 = \frac{2\psi B^2}{B_0|\nabla\psi|^2}\left\{1 + \left(\frac{|\nabla\psi|^2}{2\psi B}\right)^2\left[\int^{\eta_B}\hat{s}d\eta_B\right]^2\right\}, \tag{28}$$

$$\hat{s} = \frac{2\psi\sqrt{g_B}}{\iota}\frac{\mathbf{B}\times\nabla\psi}{|\nabla\psi|^2}\cdot\nabla\times\left[\frac{\mathbf{B}\times\nabla\psi}{|\nabla\psi|^2}\right] = s + \tilde{s}, \tag{29}$$

$$\tilde{s} = \frac{\partial}{\partial\eta_B}\left\{2\psi\frac{Jg_{\psi\theta_B} - Ig_{\psi\zeta_B}}{\sqrt{g_B}|\nabla\psi|^2}\right\}, \tag{30}$$

$$\int^{\eta_B}\hat{s}d\eta_B = s(\eta_B - \theta_k) + 2\psi\frac{Jg_{\psi\theta_B} - Ig_{\psi\zeta_B}}{\sqrt{g_B}|\nabla\psi|^2}, \tag{31}$$

$$\sqrt{g_B} = \frac{J + \iota I}{B^2}, \tag{32}$$

$$g_{\theta_B\theta_B} = \frac{\partial\mathbf{r}}{\partial\theta_B}\cdot\frac{\partial\mathbf{r}}{\partial\theta_B} = \frac{I^2 + |\nabla\psi|^2}{B^2} > 0. \tag{33}$$

For a currentless equilibria with $I = 0$, the expressions for $|\mathrm{k}_\perp|^2$, $\widetilde{s}$, and $\int^{\eta_B} \widehat{s} d\eta_B$ become especially simple:

$$|\mathrm{k}_\perp|^2 = \frac{2\psi}{B_0 g_{\theta_B\theta_B}} \left\{ 1 + \left(\frac{|\nabla\psi|}{2\psi} \right)^2 g_{\theta_B\theta_B} \left[\int^{\eta_B} \widehat{s} d\eta_B \right]^2 \right\}, \tag{34}$$

$$\widetilde{s} = \frac{\partial}{\partial \eta_B} \left\{ 2\psi \frac{g_{\psi\theta_B}}{g_{\theta_B\theta_B}} \right\}, \tag{35}$$

$$\int^{\eta_B} \widehat{s} d\eta_B = s(\eta_B - \theta_k) + 2\psi \frac{g_{\psi\theta_B}}{g_{\theta_B\theta_B}}, \tag{36}$$

where we used Eqs. (31) and (32) with $I = 0$. Note that Eqs. (33)–(35) are applicable to high-$\varepsilon\beta_p$ tokamak equilibria, because $\frac{\tau I}{J} \sim (\varepsilon_t t)^2 \ll 1$, $\frac{I^2}{|\nabla\psi|^2} \sim (\varepsilon_t t)^2 \ll 1$, and $|g_{\psi\theta_B}| \gtrsim |g_{\psi\zeta_B}|$ where $\varepsilon_t \equiv \frac{\langle r \rangle}{R}$ is the inverse aspect ratio.

We now introduce a new magnetic coordinate system $(\psi, \theta_u, \zeta_B)$ such that the toroidal angle is the same as that of the Boozer coordinate system but the poloidal angle is still arbitrary. To construct this magnetic coordinate system, the function q_T in Eq. (23) must vanish; consequently Eqs. (24) and (25) show that

$$\begin{aligned} \omega &= I\lambda_u(\psi, \theta_u, \zeta_B), \\ p_T &= \lambda_u(\psi, \theta_u, \zeta_B). \end{aligned} \tag{37}$$

Related to this new magnetic coordinate system $(\psi, \theta_u, \zeta_B)$ is a new field-line coordinate system (ψ, η_u, α_u):

$$\begin{aligned} \eta_u &= \theta_u, \\ \alpha_u &= \zeta_B - \tfrac{1}{\tau}\theta_u - \tfrac{1}{\tau}\lambda_u(\psi, \theta_u, \zeta_B). \end{aligned} \tag{38}$$

In the new field-line coordinate system, the perpendicular wave number and other associated quantities are expressed as follows:

$$|\mathrm{k}_\perp|^2 = \frac{2\psi B^2}{B_0 |\nabla\psi|^2} \left\{ 1 + \left(\frac{|\nabla\psi|^2}{2\psi B} \right)^2 \left[\int^{\eta_u} \widehat{s} d\eta_u \right]^2 \right\}, \tag{39}$$

$$\widehat{s} = \frac{2\psi\sqrt{g_u}}{t} \frac{\mathrm{B} \times \nabla\psi}{|\nabla\psi|^2} \cdot \nabla \times \left[\frac{\mathrm{B} \times \nabla\psi}{|\nabla\psi|^2} \right] = s + \widetilde{s}, \tag{40}$$

$$\tilde{s} = \frac{\partial}{\partial \eta_u}\left\{-2\psi_t \partial_\psi\left(\frac{\lambda_u}{t}\right) + 2\psi \frac{(J + I\partial_{\zeta_B}\lambda_u) g_{\psi\theta_u} - I(1+\partial_{\theta_u}\lambda_u) g_{\psi\zeta_B}}{\sqrt{g_u}|\nabla\psi|^2}\right\}, \tag{41}$$

$$\int^{\eta_u} \hat{s} d\eta_u = s(\eta_u - \theta_k) - 2\psi_t \partial_\psi\left(\frac{\lambda_u}{t}\right) + 2\psi \frac{(J + I\partial_{\zeta_B}\lambda_u) g_{\psi\theta_u} - I(1+\partial_{\theta_u}\lambda_u) g_{\psi\zeta_B}}{\sqrt{g_u}|\nabla\psi|^2}, \tag{42}$$

$$\sqrt{g_u} = \frac{1}{\nabla\psi \cdot \nabla\theta_u \times \nabla\zeta_B} = \frac{(J + tI)(1+\partial_{\theta_u}\lambda_u)}{B^2}, \tag{43}$$

$$g_{\theta_u\theta_u} = \frac{\partial \mathbf{r}}{\partial \theta_u} \cdot \frac{\partial \mathbf{r}}{\partial \theta_u} = \frac{I^2 + |\nabla\psi|^2}{B^2}(1+\partial_{\theta_u}\lambda_u)^2 > 0. \tag{44}$$

As with the Boozer coordinate system, the expressions for $|\mathbf{k}_\perp|^2$, $\tilde{s}$, and $\int^{\eta_B} \hat{s} d\eta_B$ become further simplified in the case of a currentless equilibrium ($I = 0$):

$$|\mathbf{k}_\perp|^2 = \frac{2\psi(1+\partial_{\theta_u}\lambda_u)^2}{B_0 g_{\theta_u\theta_u}}\left\{1 + \left(\frac{|\nabla\psi|}{2\psi}\right)^2 \frac{g_{\theta_u\theta_u}}{(1+\partial_{\theta_u}\lambda_u)^2}\left[\int^{\eta_u} \hat{s} d\eta_u\right]^2\right\}, \tag{45}$$

$$\tilde{s} = \frac{\partial}{\partial \eta_u}\left\{-2\psi_t \partial_\psi\left(\frac{\lambda_u}{t}\right) + 2\psi \frac{g_{\psi\theta_u}}{g_{\theta_u\theta_u}}(1+\partial_{\theta_u}\lambda_u)\right\}, \tag{46}$$

$$\int^{\eta_u} \hat{s} d\eta_u = s(\eta_u - \theta_k) - 2\psi_t \partial_\psi\left(\frac{\lambda_u}{t}\right) + 2\psi \frac{g_{\psi\theta_u}}{g_{\theta_u\theta_u}}(1+\partial_{\theta_u}\lambda_u). \tag{47}$$

The currentless condition, $I = 0$, implies that $\partial_{\zeta_B}\lambda_u$ and $g_{\psi\zeta_B}$ vanish, while the derivatives with respect to ψ and θ_u remain non-zero. For the same reason as was mentioned in connection with the Boozer coordinate system, Eqs. (44)–(46) are applicable to high-$\varepsilon\beta_p$ tokamak equilibria.

In the Boozer coordinate system, the toroidal angle ζ_B is very similar to the geometrical toroidal angle of the cylindrical coordinate system (R, φ, Z) in planar-axis heliotron/torsatron systems and tokamaks, as shown by the magnetic field line equation,

$$\frac{d\zeta_B}{d\varphi} = \frac{\mathbf{B}\cdot\nabla\zeta_B}{\mathbf{B}\cdot\nabla\varphi} = \frac{B^2 R}{(J + tI)B_\varphi} \sim \frac{B^2}{B_\varphi^2} \sim 1 + (t\varepsilon_t)^2. \tag{48}$$

Thus, if the poloidal angle is chosen subject to a mild constraint such as being proportional to the arc length, it may be possible to extract the essential parts of the local magnetic structure

from the metric elements and handle them analytically. For this magnetic coordinate system, the local rotational transform $\hat{\iota}$ is defined as

$$\hat{\iota} \equiv \frac{d\theta_u}{d\zeta_B} = \frac{\mathbf{B}\cdot\nabla\theta_u}{\mathbf{B}\cdot\nabla\zeta_B} = \iota\frac{1-q\partial_{\zeta_B}\lambda_u}{1+\partial_{\theta_u}\lambda_u}, \tag{49}$$

where $q = \frac{1}{\iota}$ is the safety factor. Although the local rotational transform $\hat{\iota}$ defined in Eq. (48) cannot be directly related to the local magnetic shear $\hat{s}$, it is still useful for obtaining an intuitive grasp of the local magnetic structure—e.g., the local compression of the poloidal field—especially if the poloidal angle θ_u is chosen such that λ_u almost vanishes in the vacuum configuration. Hereafter, we will choose θ_u as the uni-arc poloidal angle that is proportional to the arc length, taking account of results of the numerical calculations mentioned in the next section.

When the Boozer coordinate system has been given, this uni-arc magnetic coordinate system is easily constructed. The increment of the poloidal angle, $d\theta_u$, is proportional to dl_p the line element along θ_B:

$$d\theta_u \propto dl_p = \sqrt{g_{\theta_B\theta_B}}d\theta_B. \tag{50}$$

Let

$$\theta_B = \theta_u + \lambda_u(\psi,\theta_u,\zeta_B) \quad \text{or} \quad \theta_u = \theta_B - \lambda_B(\psi,\theta_B,\zeta_B), \tag{51}$$

with $\lambda_u(\psi,\theta_u,\zeta_B) = \lambda_B(\psi,\theta_B,\zeta_B)$. Then we obtain

$$\lambda_B(\psi,\theta_B,\zeta_B) = -\frac{\int_0^{\theta_B} d\theta_B\widetilde{\sqrt{g_{\theta_B\theta_B}}}}{\left\langle\sqrt{g_{\theta_B\theta_B}}\right\rangle_{\theta_B}} = -\frac{\int_0^{\theta_B} d\theta_B\left(\widetilde{\frac{|\nabla\psi|}{B}}\right)}{\left\langle\frac{|\nabla\psi|}{B}\right\rangle_{\theta_B}}, \tag{52}$$

with the average defined by

$$\langle f(\psi,\theta_B,\zeta_B)\rangle_{\theta_B} = \frac{1}{2\pi}\int_0^{2\pi} f(\psi,\theta_B,\zeta_B)d\theta_B, \tag{53}$$

and the oscillatory component given as

$$\tilde{f}(\psi,\theta_B,\zeta_B) = f(\psi,\theta_B,\zeta_B) - \langle f(\psi,\theta_B,\zeta_B)\rangle_{\theta_B}, \tag{54}$$

where Eq. (32) with the currentless condition $I = 0$ has been used. After $\lambda_B(\psi, \theta_B, \zeta_B)$ is obtained from Eq. (51), the Fourier expanded form of $\lambda_u(\psi, \theta_u, \zeta_B)$ can be expressed as

$$\lambda_u(\psi, \theta_u, \zeta_B) = \sum_{mn} \lambda_{umn}(\psi) \sin[m\theta_u - n\zeta_B], \tag{55}$$

with Fourier components

$$\begin{aligned}\lambda_{umn}(\psi) &= \frac{2}{(2\pi)^2} \int_0^{2\pi} d\theta_u \int_0^{2\pi} d\zeta_B \lambda_u(\psi, \theta_u, \zeta_B) \sin[m\theta_u - n\zeta_B], \\ &= \frac{2}{(2\pi)^2} \int_0^{2\pi} d\theta_B \int_0^{2\pi} d\zeta_B (1 - \partial_{\theta_B}\lambda_B)\lambda_B \sin[m(\theta_B - \lambda_B) - n\zeta_B].\end{aligned} \tag{56}$$

Since the Boozer toroidal angle ζ_B is similar to the geometrical toroidal angle φ, it is possible for uni-arc magnetic coordinate system $(\psi, \theta_u, \zeta_B)$ that has been introduced to be fairly similar to the VMEC magnetic coordinate system[9] $(\psi, \theta_V, \zeta_V)$, in which ζ_V is the geometrical toroidal angle and θ_V is the poloidal angle optimized to reduce the number of Fourier harmonics in the expressions for the equilibrium.

III. CHARACTERISTICS OF THE LOCAL MAGNETIC SHEAR

A. Numerical treatment

For our numerical calculations we will use $L = 2/M = 10$ planar axis heliotron/torsatron currentless equilibria like those for the Large Helical Device[8] (LHD), where L and M are the polarity and toroidal pitch number of the helical coils, respectively. The three-dimensional equilibria are calculated with the VMEC code under the condition of fixed boundary.[9] The boundary is determined from the outermost flux surface of the vacuum magnetic field, which has nearly concentric circular magnetic flux surfaces when averaged in the toroidal direction. The pressure profile given by

$$P = P_0(1 - \psi_N)^2 \tag{57}$$

is used for the numerical calculations, where $\psi_N = \frac{\psi}{\psi_{\text{edge}}}$ is the normalized toroidal flux. The normalized average minor radius $\langle r \rangle_N$ is approximately given by $\langle r \rangle_N = \sqrt{\psi_N}$. Note that

the pressure profiles obtained in experiments on the Compact Helical System[10] (CHS) are fairly close to the profile given by Eq. (56).

As shown in Fig. 1(a), the global rotational transform ι of the vacuum magnetic field monotonically increases radially outward, exceeding unity near the boundary. Hence the global magnetic shear s is positive in the whole plasma region, as shown in Fig. 1(b). This results from the inherent separatrix structure that is due to the helical coils when the global rotational transform on the separatrix $\iota_s \sim \frac{M}{L} = 5 \gg 1$. This type of vacuum ι profile is usually created by continuous helical coils, which produce a strong averaged poloidal field in their vicinity. The equally spaced (ψ, θ_B) coordinate contours in the Boozer coordinate system corresponding to the vacuum field are shown for various poloidal cross sections in Fig. 2(a). Since the vacuum field being used has on average nearly concentric circular flux surfaces in the toroidal direction, the poloidal angle θ_B of the Boozer coordinate system on each flux surface is quite similar to the poloidal angle proportional to the arc length, i.e., the uni-arc poloidal angle θ_u, apart from a weak effect due to the helicity of helical coils.

As β increases, a Shafranov shift occurs, due to the outward-directional pressure force in the major radius direction. This leads to a local compression of the poloidal magnetic field at the outer side of the torus in order to maintain toroidal force balance. Since there is no net toroidal current ($I = 0$), it is the Pfirsch-Schlüter current, $\mathbf{J} \cdot \mathbf{B}_{PS} = \mathbf{J} \cdot \mathbf{B} - \frac{\langle \mathbf{J} \cdot \mathbf{B} \rangle}{\langle B^2 \rangle} B^2$, that supports the significantly deformed flux surfaces and the modulated global and local pitch of the magnetic field, as a result of the toroidal force balance. In planar-axis heliotron/torsatron systems with small vacuum global rotational transform at the magnetic axis, the Shafranov shift in the major radius direction becomes so large (on the order of the minor radius) that it makes the flux surfaces become non-concentric on every poloidal cross section, as shown in Fig. 2(b), where the outside of the torus corresponds to the right-hand side of each figure. In correspondence with the Shafranov shift, the Pfirsch-Schlüter current localizes at the outer side of the torus on every poloidal cross section, as shown in Fig. 2(c). Thus, the

essential parts of the change in the local magnetic structure due to the Shafranov shift and the distribution of the Pfirsch-Schlüter current in planar axis heliotron/torsatron systems are axisymmetric.

In contrast to the situation with the vacuum magnetic field, the global rotational transform ι in a finite-β equilibrium increases near the magnetic axis, as indicated in Fig. 1 (a). Hence a region in which the global shear is negative ($s < 0$), as in a tokamak, appears near the magnetic axis, as shown in Fig. 1 (b). The deformation of the flux surfaces plays an essential role in changing the global rotational transform ι.[3] However, since the flux surfaces do not change very much near the plasma boundary, the value of the global rotational transform there is nearly unchanged from the vacuum field value. Thus, a shearless region ($s \sim 0$) and a region of strong positive stellarator-like global shear ($s \sim 3$) both appear, as shown in Fig. 1 (b).

The global rotational transform ι near the plasma periphery in heliotron/torsatron systems always monotonically increases in the minor radius direction, regardless of the β value, due to the strong averaged external poloidal field that is inherently created by the helical coils. By contrast, the global rotational transform in an ordinary high-$\varepsilon\beta_p$ tokamak equilibrium monotonically decreases in the direction of the minor radius. Since the Pfirsch-Schlüter current supporting the locally compressed poloidal field at the outer side of the torus is inversely proportional to the global rotational transform ι, while being proportional to $\frac{d\beta}{d\langle r\rangle}$ with $\langle r\rangle$ the average minor radius, it has a tendency to localize away from the plasma periphery in heliotron/torsatron systems (in contrast to high-$\varepsilon\beta_p$ tokamaks where it localizes near the periphery). Although the precise distribution of the Pfirsch-Schlüter current is determined by the competition of both effects, for the vacuum configuration and pressure profile used here the Pfirsch-Schlüter current flows locally around the shearless region (with minimum ι) at the outer side of the torus, as can be understood if one compares s in Fig. 1 (b) with the contours for the Pfirsch-Schlüter current in Fig. 2(c). Thus, at the

outer side of the torus, within the shearless region in the minor radius direction where the Pfirsch-Schlüter current localizes, the local and the global magnetic field structures are very similar to those for an ordinary high-$\varepsilon\beta_p$ tokamak. Outside the shearless region, however, a heliotron/torsatron system and a high-$\varepsilon\beta_p$ tokamak are very different. Specifically, the variation of the local compression of the poloidal field at the outer side of the torus is expected to be non-monotonic in the direction of the minor radius in heliotron/torsatron systems—in contrast to an ordinary high-$\varepsilon\beta_p$ tokamak equilibrium that has a monotonically decreasing rotational transform ($s < 0$). These characteristics of heliotron/torsatron systems can be clarified with the use of the Boozer poloidal angle θ_B.

In the Boozer coordinate system, because the toroidal angle ζ_B is very similar to the geometrical toroidal angle, any changes in the local magnetic field structure caused by the distribution of the Pfirsch-Schlüter current appear as a distortion of the poloidal angle θ_B. Since the Boozer poloidal angle θ_B in a vacuum configuration is substantially the same as the uni-arc poloidal angle θ_u, this distortion is represented by the quantity λ_u of Eq. (50). In the region where the poloidal magnetic field is locally strong (weak), the interval between two adjacent lines of constant θ_B becomes wide (narrow). Since this distortion results from toroidal force balance in the major radius direction, the essential parts of the distortion are axisymmetric, i.e., $\lambda_u \sim \lambda_u(\psi, \theta_u)$. Reflecting the localization of the Pfirsch-Schlüter current at the outer side of the torus, *turning points* appear on the contours of constant θ_B around the shearless surface on every poloidal cross section, as can be seen in Fig. 2(b). At such *turning points* the contours of constant θ_B and ψ become orthogonal: i.e., $g_{\psi\theta_B} = 0$. By connecting the *turning points*, we can define a *turning surface.* The contours of constant θ_B are folded back across the *turning surface.* This folding feature is conspicuous at the outer side of the torus, along with the localization of the Pfirsch-Schlüter current. Note that neither the vacuum field, shown in Fig. 2(a), nor a high-$\varepsilon\beta_p$ tokamak equilibrium with a monotonically decreasing global rotational transform has such a *turning surface.* At the outer side of the

torus, the *turning surface* divides the plasma into two separate radial domains. Inside the *turning surface*, as can be seen in Fig. 2(b), the interval between two adjacent contours of constant θ_B significantly increases radially in order to satisfy toroidal force balance, i.e., $g_{\psi\theta_B} \sim c \sin\theta_B$ with $c > 0$. Thus, in this region, the oscillatory local magnetic shear $\tilde{s}$ given by Eq. (34) is positive, whereas the global magnetic shear is negative. This situation is similar to that in a high-$\varepsilon\beta_p$ tokamak. By contrast, outside the *turning surface*, the interval between contours of constant θ_B narrows toward the plasma boundary, as can be seen in Fig. 2(b), i.e., $g_{\psi\theta_B} \sim c \sin\theta_B$ with $c < 0$. This indicates that the oscillatory magnetic shear is negative at the outer side of the torus, whereas the global magnetic shear is positive there. In other words, $\tilde{s} > 0$ in the region where $s < 0$, and vice versa. As a result, the local magnetic shear $\hat{s} = s + \tilde{s}$ becomes nearly independent of the sign of the global magnetic shear s. The integration of the oscillatory part of the local magnetic shear, $\int^{\eta_B} \tilde{s} d\eta_B = 2\psi \frac{g_{\psi\theta_B}}{g_{\theta_B\theta_B}}$, on the outer side of the torus changes sign inside and outside the *turning surface* depending on where it is performed; moreover, its sign is the opposite to that of the integrated global shear, $s\eta_B$, on both sides. This in turn leads to a reduction of the shear stabilization effect due to the field line bending term in Eq. (2), both in regions of negative and positive global shear at the outer side of the torus.

The behavior of the integrated local magnetic shear, with $\theta_k = 0$ and $\alpha = 0$, is shown in Figs. 3 and 4. The flux surfaces selected for Figs. 3 and 4 are indicated in Figs. 1 and 2 by the arrows (A) and (B) corresponding to surfaces inside and outside the *turning surface*, respectively. Figure 3 shows the behavior of the integrated local magnetic shear in the region of tokamak-like negative global magnetic shear ($s \sim -0.5$), and Fig. 4 shows the behavior in the region of strong stellarator-like global magnetic shear ($s \sim 3$). Figures 3(a) and 4(a) show the integral $\int^{\eta_B} \tilde{s} d\eta_B$ in the vacuum configuration used in Figs. 1 and 2. The same quantities are shown in Figs. 3(b) and 4(b) for a finite-β equilibrium. Clearly, the integral $\int^{\eta_B} \tilde{s} d\eta_B$ in the finite-β configuration is in phase with the toroidicity on both sides

of the *turning surface*, whereas in the vacuum configuration it is in phase with the helicity. This explains how the sign of the integral $\int^{\eta_B} \tilde{s} d\eta_B$ changes depending on the sign of the global magnetic shear. Being in phase with the toroidicity is what makes the integrated local magnetic shear $\int^{\eta_B} \hat{s} d\eta_B$ nearly vanish in the vicinity of $\eta_B = 0$, as can be shown in Fig. 4 (c). Note that the contribution of the global shear cannot be cancelled purely by the modulation due to the helicity of helical coils. Thus, the wave number $|\mathrm{k}_\perp|^2$ becomes rather small at $\eta_B = 0$ for a finite-β equilibria, as shown in Fig. 4(d), leading to a reduction of the field line bending stabilization term in Eq. (2).

B. Analytical treatment

In order to further clarify the changes in the local magnetic structure due to the Shafranov shift and to obtain a model expression for the local magnetic shear, we will use the uni-arc magnetic coordinate system $(\psi, \theta_u, \zeta_B)$ introduced in Sec. II, where θ_u is the poloidal angle proportional to the arc length defined on planes of constant ψ and ζ_B, and the toroidal angle ζ_B is the same as that in the Boozer coordinate system $(\psi, \theta_B, \zeta_B)$.

Since the Boozer poloidal angle θ_B in a vacuum configuration is very similar to the uni-arc poloidal angle and since the dominant part of the change in the local magnetic structure due to the Shafranov shift is axisymmetric, the quantity λ_u in a finite-β equilibrium may be approximated by axisymmetric components only. Then the local rotational transform $\hat{\iota}$ of the finite-β equilibrium defined in Eq. (48) may be written as

$$\hat{\iota} = \iota \frac{1}{1 + \partial_{\theta_u} \lambda_u}. \tag{58}$$

From Fig. 2(b) and Eq. (57), we see that

$$\lambda_u \sim c \sin \theta_u, \quad \text{with} \quad c < 0, \tag{59}$$

where the radial derivative $\frac{\partial c}{\partial \psi}$ is negative inside the *turning surface* and positive outside. Equations (57) and (58) show that at the outer side of the torus, the ratio of the local

rotational transform to the global rotational transform, $\frac{\hat{\iota}}{\iota}$, is a radially increasing function inside the *turning surface* where ι decreases, but that it is a radially decreasing function outside the *turning surface* where ι increases. This situation is consistent with the earlier numerical result for the local magnetic shear $\hat{s}$ described in the Boozer coordinate system.

Since the axisymmetric quantity, λ_u can be considered to be sufficient for describing the behavior of the local magnetic shear, the approximate solution of the equilibrium obtained by means of a stellarator expansion may be used in order to evaluate the quantities $|\mathbf{k}_\perp|^2$, $\tilde{s}$, and $\int^{\eta_u} \hat{s} d\eta_u$. In the uni-arc magnetic coordinate system $(\psi, \theta_u, \zeta_B)$, the quantities $|\mathbf{k}_\perp|^2$, $\tilde{s}$, and $\int^{\eta_u} \hat{s} d\eta_u$ for a currentless equilibrium are given by Eqs. (44)–(46) with the use of the axisymmetric function λ_u, i.e, $\lambda_u(\psi, \theta_u)$. The equation for a currentless equilibrium written in the stellarator expansion[11] is

$$\left[\frac{1}{r}\left(r\frac{\partial}{\partial r}\right) + \frac{1}{r^2}\frac{\partial^2}{\partial \theta^2}\right]\chi = -R_0^2 \frac{d\beta}{d\chi}\frac{r\cos\theta}{R_0} + \frac{1}{r}\frac{d}{dr}\left[r^2 \iota_v(r)\right], \tag{60}$$

where $\chi \equiv \frac{\Phi_p}{2\pi B_0}$ with Φ_p the poloidal flux, $\beta \equiv \frac{2P(\chi)}{B_0^2}$, and B_0 is the strength of the magnetic field at $R = R_0$. A quasi-toroidal coordinate system (r, θ, φ) with clockwise θ is used, which is related to the cylindrical coordinate system (R, φ, Z) as follows:

$$\begin{aligned} R &= R_0 + r\cos\theta, \quad 0 \le r \le a, \\ Z &= \quad -r\sin\theta. \end{aligned} \tag{61}$$

Since the vacuum field considered here has concentric circular magnetic flux surfaces, the plasma boundary is assumed to be a circle of radius $r = a$, and the vacuum field in Eq. (59) is assumed to be helically symmetric, so that the vacuum poloidal flux can be expressed in terms of the vacuum rotational transform ι_v, which is a function of r, as may be seen from the second term on the right-hand side of Eq. (59). The currentless equilibrium can be approximately solved with the use of the so-called Shafranov coordinate system[12] (r_s, θ_s, ζ_s),

which is defined by

$$\begin{aligned} r\cos\theta &= \Delta(r_s) + r_s\cos\theta_s, \\ r\sin\theta &= r_s\sin\theta_s, \\ \varphi &= \zeta_s, \end{aligned} \tag{62}$$

with Δ the Shafranov shift. In the Shafranov coordinate system (r_s, θ_s, ζ_s), the magnetic flux surfaces are assumed to be non-concentric circles of minor radius r_s, whose center is determined by the Shafranov shift $\Delta(r_s)$ for each surface from the relation $(r,\theta) = (\Delta(r_s), 0)$. The Shafranov shift Δ has the following properties:

$$\Delta(r_s) \geq 0, \quad \Delta(a) = 0, \quad \Delta'(r_s) \leq 0, \equiv \frac{d}{dr_s}. \tag{63}$$

Thus, the normalized poloidal flux function $\chi = \chi(r_s)$ is assumed to be a function of r_s. In the Shafranov coordinate system (r_s, θ_s, ζ_s), the equation for a currentless equilibrium of Eq. (59) is given by

$$\frac{1}{r_s X}\frac{\partial}{\partial r_s}\left(\frac{r_s^2}{X}\iota\right) + \frac{\iota\Delta'}{X}\frac{\partial}{\partial\theta_s}\left(\frac{\sin\theta_s}{X}\right) = -R_0^2\frac{\beta'}{r_s\iota}\frac{\Delta + r_s\cos\theta_s}{R_0} + \frac{1}{r}\frac{d}{dr}(r^2\iota_v(r)). \tag{64}$$

Here we define

$$\begin{aligned} X &= 1 + \Delta'\cos\theta_s, \\ |\nabla r_s|^2 &= \frac{1}{X^2}, \quad \nabla r_s\cdot\nabla\theta_s = \frac{\Delta'\sin\theta_s}{r_s X^2}, \\ \sqrt{g_s} &= \frac{1}{\nabla r_s\times\nabla\theta_s\cdot\nabla\zeta_s} = R_0 r_s X, \end{aligned} \tag{65}$$

and the following relation[11] was used:

$$\iota(r_s) = \left[\frac{1}{2\pi}\int_0^{2\pi}\frac{r_s d\theta_s}{|\nabla\chi|}\right]^{-1} = \frac{\chi'}{r_s}. \tag{66}$$

From Eq. (63), we see that $r_s = r$ and $\iota(r_s) = \iota_v(r)$ for the vacuum magnetic field with $\beta = 0$ and $\Delta \equiv 0$. Since the Boozer toroidal angle is very similar to the geometrical toroidal angle and since the poloidal angles in the Shafranov and uni-arc coordinate systems are both

proportional to the arc length, we could treat the Shafranov coordinate system (r_s, θ_s, ζ_s) as a uni-arc magnetic coordinate system $(\psi, \theta_u, \zeta_B)$.

Thus, by evaluating Eq. (43) with $I = 0$ in the Shafranov coordinate system, we obtain the following relation:

$$1 + \partial_{\theta_s}\lambda_s = \sqrt{g_{\theta_s\theta_s}}\frac{B}{|\nabla\psi_s|} = X = 1 + \Delta' \cos\theta_s, \tag{67}$$

where

$$\sqrt{g_{\theta_s\theta_s}} = r_s, \quad B \sim B_0, \quad \psi_s \sim \frac{B_0 r_s^2}{2} \tag{68}$$

are used. Therefore we have

$$\lambda_s = \Delta'(r_s)\sin\theta_s. \tag{69}$$

From Eq. (50) and the relation given by Eq. (68), we see that the difference between the poloidal angle in the Boozer coordinate system and that in the uni-arc (Shafranov) coordinate system is approximately proportional to the derivative of the Shafranov shift:

$$\theta_B \sim \theta_s + \Delta'(r_s)\sin\theta_s = \int_0^{\theta_s} \frac{\iota}{\hat{\iota}} d\theta_s, \tag{70}$$

where

$$\hat{\iota} = \frac{\mathbf{B}\cdot\nabla\theta_s}{\mathbf{B}\cdot\nabla\zeta_s} = \iota\frac{1}{1 + \Delta'(r_s)\cos\theta_s}. \tag{71}$$

For a vacuum magnetic field where the Boozer poloidal angle θ_B is similar to the uni-arc poloidal angle θ_s, the Boozer poloidal angle θ_B deviates from θ_s as β increases through Δ'. The deviation of θ_B from θ_s corresponds to the deviation of the local rotational transform $\hat{\iota}$ from the global rotational transform ι. Thus, it can be understood that the radial profile of θ_B and $\hat{\iota}$ reflect how the toroidal force balance is maintained, i.e., how the local compression of the poloidal field on the outer side of the torus occurs through the derivative of the Shafranov shift, Δ'. By using Eqs. (64), (67), and (68) and the relation

$$g_{\psi_s\theta_s} = -\frac{\Delta'}{B_0}\sin\theta_s, \tag{72}$$

we can rewrite Eqs. (44) and (46) as

$$|\mathrm{k}_\perp|^2 = (1+\Delta'\cos\theta_s)^2\left\{1+\left[\frac{\int^{\theta_s}\widehat{s}d\theta_s}{(1+\Delta'\cos\theta_s)^2}\right]^2\right\}, \tag{73}$$

$$\widetilde{s} = \frac{\partial}{\partial\theta_s}\left\{-\Delta'\left[1+\Delta'\cos\theta_s - s + \frac{r_s\Delta''}{\Delta'}\right]\sin\theta_s\right\}, \tag{74}$$

$$\int^{\theta_s}\widehat{s}d\theta_s = s(\theta_s-\theta_k) - \Delta'\left[1+\Delta'\cos\theta_s - s + \frac{r_s\Delta''}{\Delta'}\right]\sin\theta_s, \tag{75}$$

where η_s has been replaced by θ_s. Thus, the qualitative properties of the quantities $|\mathrm{k}_\perp|^2$, $\widetilde{s}$, and $\int^{\eta_s}\widehat{s}d\eta_s$ can be understood from consideration of the Shafranov shift $\Delta(r_s)$. For this purpose Eq. (63) may be solved with the use of an expansion around the magnetic axis,[13] which is justified by the ordering $\beta = O(\varepsilon_t)$ in the stellarator expansion. This ordering corresponds to the high-β ordering for a tokamak equilibrium, and hence we cannot assume $\Delta' = O(\varepsilon_t)$ as is done in the low-β ordering for a tokamak equilibrium when the model equation for high-mode-number ballooning modes in a tokamak is derived. Moreover, for simplicity, the vacuum rotational transform ι_v will be assumed to be nearly shearless. By expanding the equilibrium quantities as

$$\begin{aligned}
\iota &= \iota_0 + \iota_2 r_s^2 + \iota_4 r_s^4 + \cdots, \\
\Delta &= \Delta_0 + \Delta_2 r_s^2 + \Delta_4 r_s^4 + \cdots, \\
\beta &= \beta_0 + \beta_2 r_s^2 + \beta_4 r_s^4 + \cdots,
\end{aligned} \tag{76}$$

and substituting the above quantities into Eq. (63), we find that the lowest order expanded form of Eq. (63) is given by

$$2\iota_0 - 8\Delta_2\iota_0 r_s\cos\theta_s + \cdots = -\frac{2R_0\Delta_0\beta_2}{\iota_0} + 2\iota_v - \frac{2R_0\beta_2}{\iota_0}r_s\cos\theta_s + \cdots. \tag{77}$$

Thus, two independent relations are obtained from the $\cos\theta_s$-independent and the $\cos\theta_s$-dependent terms:

$$\iota_0 = -\frac{R_0\Delta_0\beta_2}{\iota_0} + \iota_v, \tag{78}$$

$$2\Delta_2\iota_0 r_s = \frac{R_0}{4\iota_0} 2\beta_2 r_s. \tag{79}$$

Both relations may be thought of as the form of the following two relations expanded about the magnetic axis:

$$\iota = -\frac{R_0\Delta\beta''}{2\iota} + \iota_v, \tag{80}$$

$$\Delta' = \frac{R_0}{4\iota^2}\beta' < 0. \tag{81}$$

We have assumed that the monotonically decreasing pressure profile determines the sign of Eq. (80). Equation (80) indicates that $\Delta' = O(1)$ for the stellarator-ordering $\beta = O(\varepsilon_t)$. According to Eq. (79), we see that ι increases compared with ι_v near the magnetic axis with $\beta'' < 0$, but decreases near the plasma periphery with $\beta'' > 0$. Also, the flux surface at which $\iota = \iota_v$ holds is determined by the pressure profile, independent of the β value. These changes in the global rotational transform ι when β increases are always seen in numerical calculations of the 3D equilibrium considered here.[14] Therefore, although Eqs. (79) and (80) are obtained by an expansion around the magnetic axis, we may consider these two relations to have the form that is reasonably applicable over the entire plasma region except for the region very near the plasma boundary, at least for the purpose of a qualitative investigation of the local magnetic shear $\hat{s}$ and the perpendicular wave number $|\mathbf{k}_\perp|$. Because we have

$$\Delta'' = \frac{R_0}{4\iota^2}\left[-\frac{2\iota'}{\iota}\beta' + \beta''\right], \tag{82}$$

from Eq. (80), we can understand that λ_s and Δ', given by Eqs. (68) and (80), respectively, satisfy the qualitative property given by Eq. (58), because $\iota' < 0$ and $\beta'' < 0$ near the magnetic axis and $\iota' > 0$ and $\beta'' > 0$ near the plasma periphery.

In order to compare the results obtained here with the standard results due to the steep-gradient model in a low-β tokamak equilibrium, we introduce new variables:

$$s_q = \frac{r_s}{q}\frac{dq}{dr_s} = -s, \quad \tilde{s}_q = -\tilde{s}, \quad \hat{s}_q = -\hat{s}, \tag{83}$$

$$\alpha = -\Delta' = -\frac{R_0}{4\iota^2}\beta' > 0. \tag{84}$$

By substituting those new variables into Eqs. (72)–(74), we find

$$|\mathrm{k}_\perp|^2 = (1-\alpha\cos\theta_s)^2\left\{1+\left[\frac{\int_0^{\theta_s}\hat{s}_q d\theta_s}{(1-\alpha\cos\theta_s)^2}\right]^2\right\}, \tag{85}$$

$$\begin{aligned}\tilde{s}_q &= \frac{\partial}{\partial\theta_s}\left\{-\alpha\left[1-\alpha\cos\theta_s+s_q+\frac{r_s\alpha'}{\alpha}\right]\sin\theta_s\right\} \\ &= \frac{\partial}{\partial\theta_s}\left\{-\alpha\left[1-\alpha\cos\theta_s+3s_q+\frac{r_s\beta''}{\beta'}\right]\sin\theta_s\right\},\end{aligned} \tag{86}$$

$$\begin{aligned}\int_0^{\theta_s}\hat{s}_q d\theta_s &= s_q(\theta_s-\theta_k)-\alpha\left[1-\alpha\cos\theta_s+s_q+\frac{r_s\alpha'}{\alpha}\right]\sin\theta_s \\ &= s_q(\theta_s-\theta_k)-\alpha\left[1-\alpha\cos\theta_s+3s_q+\frac{r_s\beta''}{\beta'}\right]\sin\theta_s,\end{aligned} \tag{87}$$

where β'' enters through Eq. (81). Note that the correction terms $3s_q+\frac{r_s\beta''}{\beta'}$ due to the global magnetic shear and pressure exist in the oscillatory part of the local magnetic shear $\tilde{s}$. Simplified forms of Eqs. (84)–(86), with only the essential terms kept, are given by

$$|\mathrm{k}_\perp|^2 = 1+\left[\int_0^{\theta_s}\hat{s}_q d\theta_s\right]^2, \tag{88}$$

$$\tilde{s}_q = -\alpha\left[1+3s_q+\frac{r_s\beta''}{\beta'}\right]\cos\theta_s, \tag{89}$$

$$\int_0^{\theta_s}\hat{s}_q d\theta_s = s_q(\theta_s-\theta_k)-\alpha\left[1+3s_q+\frac{r_s\beta''}{\beta'}\right]\sin\theta_s. \tag{90}$$

Equations (84)–(89) are applicable to a high-$\varepsilon\beta_p$ tokamak. Indeed, Eqs. (84)–(86) are exactly same as those in Ref. 13, except for the terms related to β in Eqs. (85) and (86), although the

model equation for high-mode-number ballooning modes in a high-$\varepsilon\beta_p$ tokamak equilibrium is derived with the use of a different coordinate system.

At the outer side of the torus ($\theta_s \sim 0$), Eq. (89) can be written, for $\theta_k = 0$, as

$$\int_0^{\theta_s} \hat{s}_q d\theta_s = \left[s_q - \alpha \left(1 + 3s_q + \frac{r_s \beta''}{\beta'} \right) \right] \theta_s. \tag{91}$$

For a monotonically decreasing pressure profile like the one given by Eq. (56), $\frac{r_s\beta''}{\beta'}$ is positive near the magnetic axis and negative near the plasma periphery. Define

$$\beta = \beta_0 f(r_s), \tag{92}$$

where $f(r_s)$ is a given function of r_s; then the critical pressure at which the stabilizing effects of the local magnetic shear disappear is given by

$$\beta_{0c} = -\frac{4\iota^2}{R_0 f'} \frac{s_q}{1 + 3s_q + \frac{r_s f''}{f'}}. \tag{93}$$

For the ordinary high-$\varepsilon\beta_p$ tokamaks with a monotonically decreasing global rotational transform, i.e., $s_q > 0$, a result is obtained that is qualitatively similar to the usual model for the local magnetic shear in the steep-gradient model for a low-β tokamak equilibrium: namely, pressure values for which $\beta_0 \ll \beta_{0c}$ is satisfied correspond to the first stable region. For pressures such that $\beta_0 \sim \beta_{0c}$, high-mode-number ballooning modes become unstable. The second stable region is attained when the pressure satisfies $\beta_0 \gg \beta_{0c}$. The physical meaning of the global shear correction term in the oscillatory component of the local magnetic shear $\tilde{s}$ is as follows: An ordinary tokamak equilibrium has a monotonically decreasing global rotational transform, i.e., a monotonically decreasing averaged poloidal field. The faster the averaged poloidal field decreases in the direction of the minor radius , i.e., the larger the global shear s_q is, the stronger the local compression of the poloidal magnetic field that is needed at the outer side of the torus to maintain toroidal force balance. The above physical mechanism appears in the oscillatory component of the local magnetic shear $\tilde{s}_q$ by enhancing the coefficient of the α term in Eqs. (86), (89), and (90).

For a high-$\varepsilon\beta_p$ tokamak with reversed magnetic shear ($s_q < 0$) near the magnetic axis, at first sight it might be thought that it is possible for the local magnetic shear $\widehat{s}_q$ to vanish. Near the magnetic axis, however, the pressure correction term $\frac{r_s\beta''}{\beta'}$ is positive and the global magnetic shear s_q is weak, so that the integrated oscillatory local magnetic shear does not change sign, i.e., $1 + 3s_q + \frac{r_s\beta''}{\beta'} > 0$.

In contrast with a high-$\varepsilon\beta_p$ tokamak with reversed magnetic shear, in heliotron/torsatron systems the global magnetic shear is so strong in the stellarator-like global magnetic shear region, as shown in Fig. 1(b), that the oscillatory component of the local magnetic shear can change sign. From Eqs. (56) and (89), the correction term $1 + 3s_q + \frac{r_s\beta''}{\beta'}$ is positive in the tokamak-like global shear region and negative in the stellarator-like global shear region. This behavior is consistent with Figs. 3(b) and 4(b), respectively. The physical meaning of the global shear correction term in the oscillatory component of the local magnetic shear $\widetilde{s}$ is now manifest. Near the plasma periphery of a heliotron/torsatron system, the averaged poloidal field due to the helical coils monotonically increases up to over unity, i.e., the global rotational transform monotonically increases. The faster the averaged poloidal field increases in the direction of the minor radius, i.e., the smaller the global shear s_q is, the stronger the local compression (enhancement) of the poloidal magnetic field that is needed to maintain toroidal force balance is suppressed at the outer side of the torus. This physical mechanism appears in the oscillatory component of the local magnetic shear $\widetilde{s}_q$ by reducing the coefficient of the α term in Eqs. (86), (89), and (90).

The critical pressure (or critical pressure gradient) in the strong stellarator-like global magnetic shear region is given by

$$\beta_{0c} \sim -\frac{4\iota^2}{3R_0 f'} \quad \text{or} \quad -\beta_c' \sim \frac{4\iota^2}{3R_0}, \tag{94}$$

where $1 + 3s_q + \frac{r_s\beta''}{\beta'} \sim 3s_q$ was used in Eq. (92).

IV. DISCUSSION

We have investigated the properties of the local magnetic shear in heliotron/torsatron systems with a large Shafranov shift. There is a possibility that the local magnetic shear vanishes, independent of the sign of the global magnetic shear. The physical reason for this comes from the fact that the degree of the local compression of the poloidal magnetic field at the outer side of the torus to maintain the toroidal force balance is strongly dependent on the magnitude of the global rotational transform (i.e., the averaged poloidal field). When the global rotational transform (averaged poloidal field) decreases in the minor radius direction, i.e., the global magnetic shear is negative as in usual tokamaks (in our definition), the degree of the local compression of the poloidal field at the outer side of the torus must increase in the minor radius direction, since otherwise toroidal force balance can not be maintained. In contrast, when the global rotational transform (averaged poloidal field) increases in the minor radius direction, i.e., the global magnetic shear is positive, the degree of the local compression of the poloidal field outside of the torus does not have to increase in the minor radius direction. Rather, it must decrease, because the larger the global rotational transform (averaged poloidal field) becomes, the less the local compression of the poloidal field that is needed to maintain toroidal force balance. Thus, the degree of the local compression decreases (increases) radially outward when the global rotational transform increases (decreases) radially outward, leading the local magnetic shear to be reduced or to even vanish, independent of the sign of the global magnetic shear.

Since the Shafranov shift and the related local compression of the poloidal field at the outer side of the torus come from the outward pressure force in the major radius direction, they are inherently axisymmetric. Thus, the reduction or vanishing of the local magnetic shear is not strongly dependent on the label of the magnetic field lines.

Although there are many variations for the vacuum magnetic configuration in the he-

liotron/ torsatron system considered here, having to maintain toroidal force balance (local compression of the poloidal field outside of the torus) and having a monotonically increasing ι profile near the plasma periphery that essentially comes from the external magnetic field due to the helical coils are both common features to all cases. Therefore, the reduction or the vanishing of the local magnetic shear in the stellarator-like positive global magnetic shear region will occur, independent of the particular vacuum configurations.

The pressure profile has a significant effect on the magnitude of the Shafranov shift and the profile of the global rotational transform, leading to changes in both the position where the Pfirsch-Schlüter current is localized and the position of the *turning surface.* However, since a monotonically increasing global rotational transform still exists near the plasma periphery independent of the pressure profile, the reduction or vanishing of the local magnetic shear in the stellarator-like global magnetic shear region will more or less occur, although the β value at which the disappearance will occur may be different.

Note that the vanishing of the local magnetic shear in the stellarator-like global magnetic shear region is universal in $L = 2$ heliotron/torsatron systems that have a large Shafranov shift because it is caused by toroidal force balance in the stellarator-like global shear region that is inherent to such the systems.

The stability characteristics of the high-mode-number ballooning modes,[15] which mirror the properties of the local magnetic shear, will be examined in a companion paper, along with the characteristics of the local magnetic curvature. In accordance with the α-dependence that stems from the nature of the local magnetic curvature, the high-mode-number ballooning modes in heliotron/torsatron systems can be classified into two types: One is tokamak-like, while the other is inherent to heliotron/torsatron systems. The relation of the high-mode-number ballooning modes to the low-mode-number modes are also discussed.

The model equations for the (integrated) local magnetic shear and the perpendicular wave

number can be used to construct the model equation for the high-mode-number ballooning modes in heliotron/torsatron systems, which will be mentioned elsewhere.

ACKNOWLEDGMENTS

The author expresses his gratitude to Professors M. Okamoto and T. Sato of the National Institute for Fusion Science and to Professor R.D. Hazeltine of the Institute for Fusion Studies for their interest in and encouragement of this work. The author also would like to thank Professors H.L. Berk and J.W. Van Dam of the Institute for Fusion Studies for fruitful discussions and their interest in this work.

The author's work was supported by AFOSR grant F49620-95-1-0529 through the Japan Industry and Management of Technology (JIMT) Program at the IC^2 Institute, The University of Texas at Austin. It was also partially supported by the U.S. Department of Energy under contract DE-FG03-96ER-54346 with the Institute for Fusion Studies. The author's visit was arranged through the U.S.-Japan Joint Institute for Fusion Theory exchange program.

References

[1] V.D. Shafranov, Phys. Fluids **26**, 357 (1983).

[2] H.L. Berk, M.N. Rosenbluth, and J.L. Shohet, Phys. Fluids **26**, 2616 (1983).

[3] X. Llobet, H.L. Berk, and M.N. Rosenbluth, Phys. Fluids **30**, 2750 (1987).

[4] W.A. Cooper, S.P. Hirshman, D.K. Lee, Nucl. Fusion **29**, 617 (1989).

[5] J.M. Greene, J.L. Johnson, Plasma Phys. **10**, 729 (1968).

[6] A.H. Boozer, Phys. Fluids **23**, 904 (1980).

[7] R.D. Hazeltine and J.D. Meiss, Phys. Reports **121**, 1 (1985).

[8] A. Iiyoshi, M. Fujiwara, O. Motojima, N. Oyabu, and K. Yamazaki, Fusion Technol. **17**, 148 (1990).

[9] S.P. Hirshman, Phys. Fluids **26**, 3553 (1983).

[10] S. Okamura, K. Matsuoka, K. Nishimura, K. Tsumori, R. Akiyama, S. Sakakibara, H. Yamada, S. Morita, T. Morisaki, N. Nakajima, K. Tanaka, J. Xu, K. Ida, H. Iguchi, A. Lazaros, T. Ozaki, H. Arimoto, A. Ejiri, M. Fujiwara, H. Idei, O. Kaneko, K. Kawahata, T. Kawamoto, A. Komori, S. Kubo, O. Motojima, V.D. Pustovitov, C. Takahashi, K. Toi, and I. Yamada, Nucl. Fusion **35**, 283 (1995).

[11] G. Anania, J.L. Johnson, and K.E. Weimer, Phys. Fluids **26**, 2210 (1983).

[12] V.D. Shafranov, in *Reviews of Plasma Physics*, ed. M.A. Leontovich (Consultants Bureau, New York, 1966), Vol. 2, p. 103.

[13] B. Coppi, A. Ferreira, J.W.-K. Mark, and J.J. Ramos, Nucl. Fusion **19**, 715 (1979).

[14] K. Ichiguchi, N. Nakajima, M. Okamoto, Y. Nakamura, and M. Wakatani, Nucl. Fusion **33**, 481 (1993).

[15] R.L. Dewar and A.H. Glasser, Phys. Fluids **26**, 3038 (1983).

FIGURE CAPTIONS

FIG. 1. Radial profiles of (a) the global rotational transform ι and (b) the global magnetic shear s, for a vacuum (dot-dashed curves) and a finite-β (solid curve) $L = 2/M = 10$ heliotron/torsatron system. The β value at the magnetic axis of the finite-β equilibrium is 7%.

FIG. 2. (a) Equally spaced (ψ, θ_B) mesh on several poloidal cross sections for the vacuum configuration in Fig. 1; (b) equally spaced (ψ, θ_B) mesh for the finite-β equilibrium in Fig. 1; and (c) corresponding contours for the Pfirsch-Schlüter current: $(\mathbf{J}\cdot\mathbf{B}_{PS} \equiv \mathbf{J}\cdot\mathbf{B} - \langle \mathbf{J}\cdot\mathbf{B}\rangle \frac{B^2}{\langle B^2\rangle})$. The center axis of the torus is on the left-hand side of each figure, so that the outer side of the torus corresponds to the right-hand side of each figure. The directions of the poloidal angle and magnetic field lines are clockwise and the direction of the Pfirsch-Schlüter current is from the front to the back of the paper ($+\zeta$ direction) in the region drawn by thick curves. The position of $\theta_B = 0$ is on the equatorial plane outside the torus.

FIG. 3. Variations along the field line in the tokamak-like global magnetic shear region indicated by the arrow (a) in Figs. 1 and 2 of: (a) $\int^{\eta_B} \tilde{s} d\eta_B$ in the vacuum configuration of Figs. 1 and 2, (b) $\int^{\eta_B} \tilde{s} d\eta_B$ in the finite-β equilibrium of Figs. 1 and 2, (c) $\int^{\eta_B} \hat{s} d\eta_B$ and $s\eta_B$ (thin line) in the finite-β equilibrium of Figs. 1 and 2, (d) $|\mathrm{k}_\perp|^2$ in the finite-β equilibrium of Figs. 1 and 2. The position $\eta_B = 0$ corresponds to the equatorial plane at the outer side of the torus in the horizontally elongated cross section of Fig. 2.

FIG. 4. The same quantities as in Fig. 3 in the stellarator-like global magnetic shear region indicated by the arrow (b) in Figs. 1 and 2.

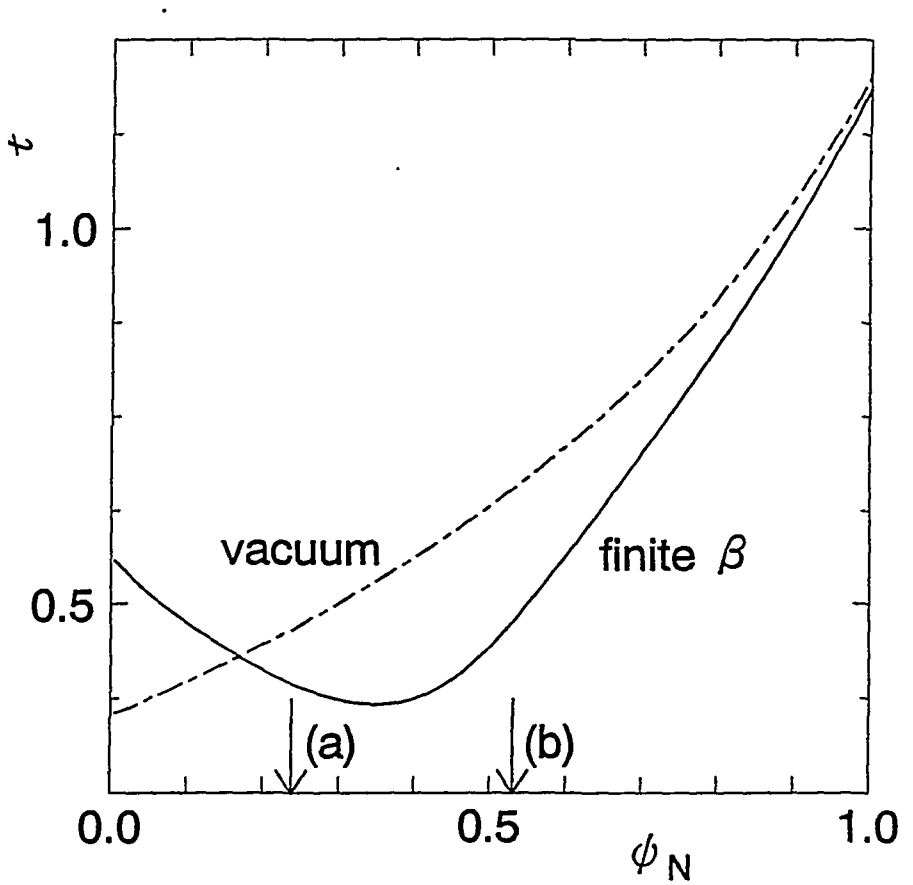

Fig. 1(a)

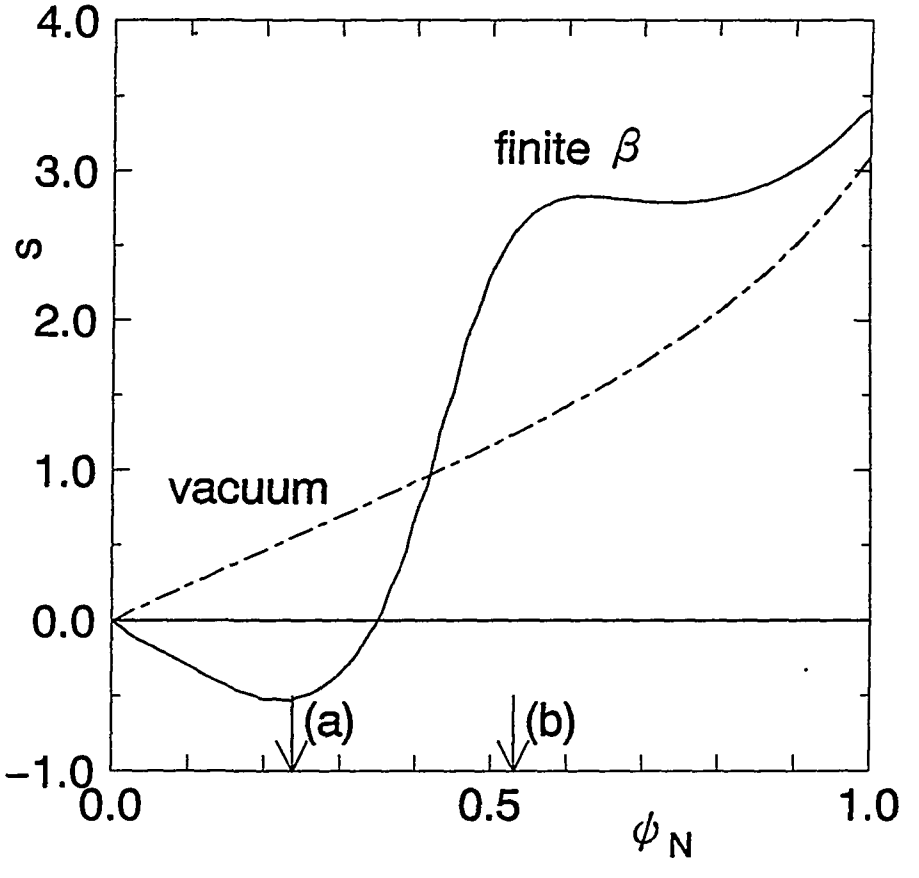

Fig. 1(b)

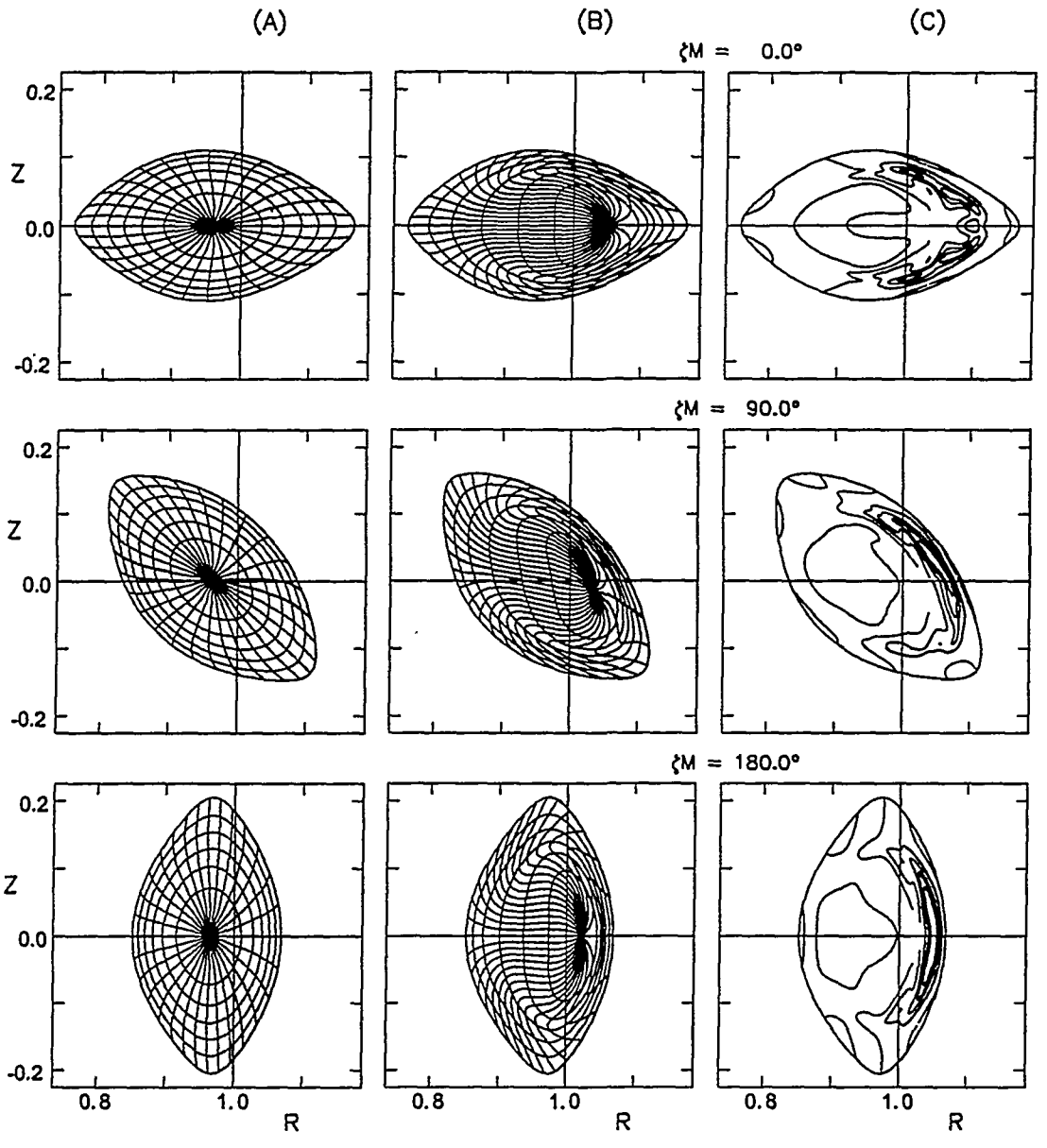

Fig. 2

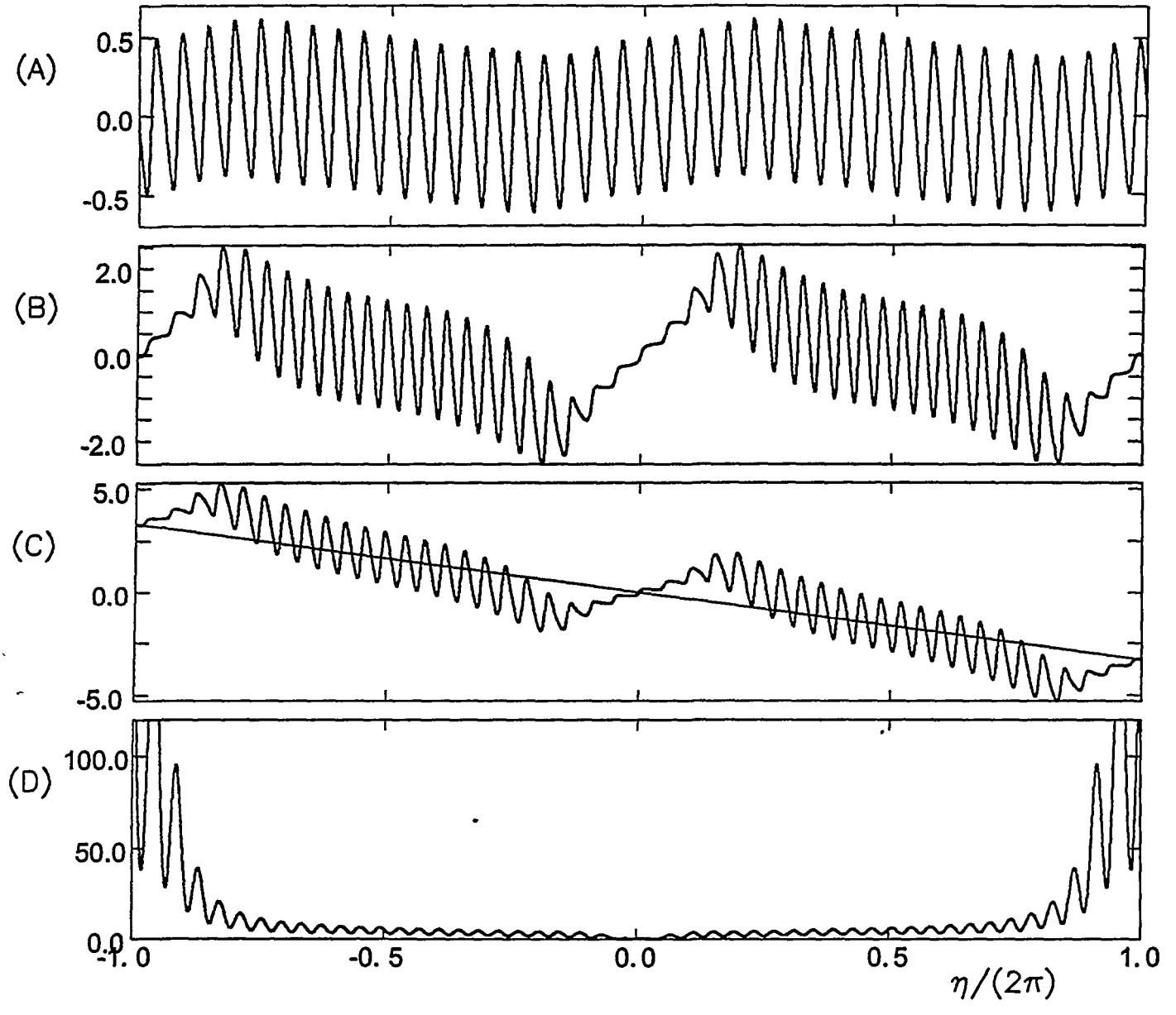

Fig. 3

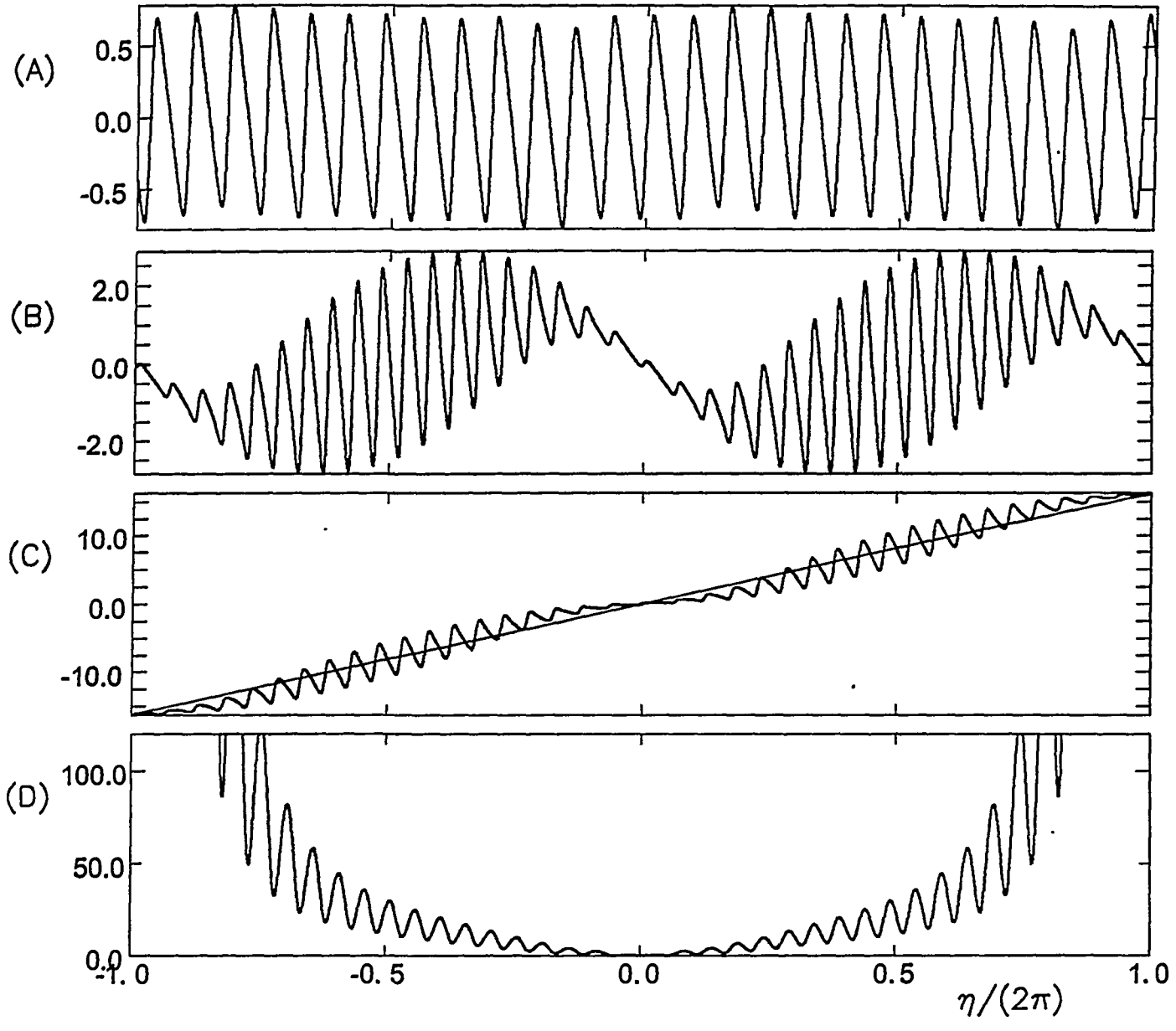

Fig. 4